S & M 4566

Effect of Sediment Flux on Cs-137 Dispersion in the Yellow and East China Seas: Case Study Using the POSEIDON-R Box Model

Hanna Kim, Seongbong Seo, Kyeong Ok Kim,*
Young-Il Kim, Myoung Hoon Lee, and Hyung-Gyu Lim

Korea Institute of Ocean Science & Technology
(49111) KIOST, 385, Haeyang-ro, Yeongdo-gu, Busan Metropolitan City, Korea

(Received November 21, 2025; accepted July 24, 2026)

Keywords: Cs-137, radionuclide, sediment flux, suspended sediment, POSEIDON-R box model

A POSEIDON-R box model was applied to the Yellow and East China Seas to assess the role of sediment flux in the fate of Cs-137. Key parameters, including suspended sediment concentration, sediment flux, bioturbation intensity, top sediment layer thickness, and porosity, were updated with recent field and satellite data. Atmospheric deposition was reconstructed from Global Precipitation and in situ measurements and imposed as a time-dependent input. Although the model reproduced the overall observed trends, it consistently underestimated Cs-137 concentrations in both water and surface sediments when the observational sediment flux data were used. Three sensitivity tests were performed: (1) the re-estimation of sediment fluxes, (2) the application of differentiated sediment fluxes (settling velocities) between the water column and the sediment layer, and (3) the incorporation of observed distribution coefficients (K_d) into the model. The model responses were quantitatively assessed to determine the contributions of each parameter individually. The adjustment of sediment fluxes led to partial improvement in model performance within both the seawater and sediment layers; however, Cs-137 concentrations in both compartments remained underestimated compared with observations. In contrast, applying differentiated sediment fluxes to the seawater and sediment layers significantly enhanced model reproducibility. In addition, the application of observed K_d values improved the accuracy of Cs-137 predictions in the sediment layer, particularly in the Yellow Sea. These results highlight the importance of accurately characterizing both sediment flux and K_d, especially in high-turbidity regions such as the Yellow and East China Seas, to enhance model performance. However, the limited availability of reliable sediment flux and K_d data remains a limitation of this study. This study also demonstrates the importance of sensor-based observational data for improving the parameterization and predictive capability of marine radioactivity models.

*Corresponding author: e-mail: kokim@kiost.ac.kr
https://doi.org/10.18494/SAM6202

ISSN 0914-4935

1. Introduction

Since the Fukushima Daiichi Nuclear Power Plant (FDNPP) accident in 2011, numerous studies have been conducted to quantitatively understand and predict radionuclide behavior in marine environments and their transfer processes within marine biota. Among the various modeling approaches, the POSEIDON-R model has been widely applied owing to its capability to comprehensively simulate the transport and accumulation of radionuclides among the water column, sediments, and marine organisms.

This numerical model is specifically designed for marine radioactivity transfer simulations, providing an integrated framework for evaluating radionuclide dynamics in marine ecosystems. Maderich *et al.*(1) developed a box model system for the northwestern Pacific Ocean and applied the POSEIDON-R model, incorporating a pelagic food web module, to simulate the behavior of Cs-137 in seawater, sediments, and marine biota. A comparison with observational data from 1945 to 2010 demonstrated good model performance in major regional seas surrounding the Korean Peninsula, including the East China and Yellow Seas.

Subsequently, Bezhenar *et al.*(2) extended the original model by introducing a benthic food web, thereby developing the Extended BURN model consisting of 11 functional groups. Using this enhanced model, they validated Cs-137 distributions in the water column, sediments, and marine organisms in the vicinity of the Fukushima box. Although this study provided valuable insights into the role of contaminated sediments in radionuclide transfer, model validation for the Korean coastal waters had not been performed.

Maderich *et al.*(3) further refined the approach by introducing a resuspension mechanism into a 108-box model system for the northeastern Atlantic continental shelf, simulating Cs-137 dynamics from 1950 to 2040. Their results demonstrated that accounting for sediment resuspension significantly improved the predictive accuracy of the model.

In a more recent study, Kim *et al.*(4) re-evaluated several key parameters of the POSEIDON-R model—including suspended sediment concentration, sediment flux, bioturbation intensity, top sediment layer thickness, and porosity—to enhance the model's predictive performance by incorporating region-specific characteristics. However, the model tended to underestimate Cs-137 concentrations in the water column and sediments of the Yellow and East China Seas. This discrepancy was attributed to the excessive accumulation of radionuclides in bottom sediments, which resulted from applying identical settling velocities to both the water column and sediment layers; these velocities were significantly higher than in previous simulations, thereby amplifying this effect.

To improve the underestimation issue of Cs-137 concentrations in these regions, the present study considers three main approaches. First, the suspended sediment flux was re-evaluated on the basis of updated field observations. Second, the physical differentiation between settling velocities in the water column and within the sediment layer was incorporated to better represent realistic particle dynamics and reduce excessive sedimentation. Third, experimentally observed K_d values were implemented to more accurately capture the partitioning behavior between the particulate and dissolved phases of radionuclides.

By comparing the simulation results of the modified POSEIDON-R model with observational data, in this study, we aim to comprehensively assess the behavior of radionuclides in regions with active resuspension and evaluate the model's predictive performance under different parameterization schemes.

2. Materials and Methods

In this section, we provide a concise description of the model framework, with particular emphasis on sediment flux and suspended sediment concentration, along with the input datasets and the observational data used for model validation.

2.1 POSEIDON-R model description

In this study, the POSEIDON-R 3D compartment model utilized for marine radioactivity assessments was applied to predict the radiological impacts in the marine environment. The model incorporates both the pelagic and benthic biological components and focuses on simulating the transport behavior of the radionuclide Cs-137 in seawater and sediment compartments. The model is composed of up to three layers in the water column and three sections in the sediment layers, allowing the representation of radionuclide transport processes within and between these compartments, as illustrated in Fig. 1(a).

In the water column, the model simulates radionuclide transport driven by water exchange between adjacent boxes, which is parameterized using water fluxes defined between layers and boxes, including interactions between boxes with different vertical structures, vertical diffusion among layers, and interactions between the water and sediment layers, including particle settling and bioturbation. The mathematical formulation of these processes is presented in Eq. (1), while Eqs. (2) and (3) describe the radionuclide transport dynamics in the upper and middle sediment layers, respectively.

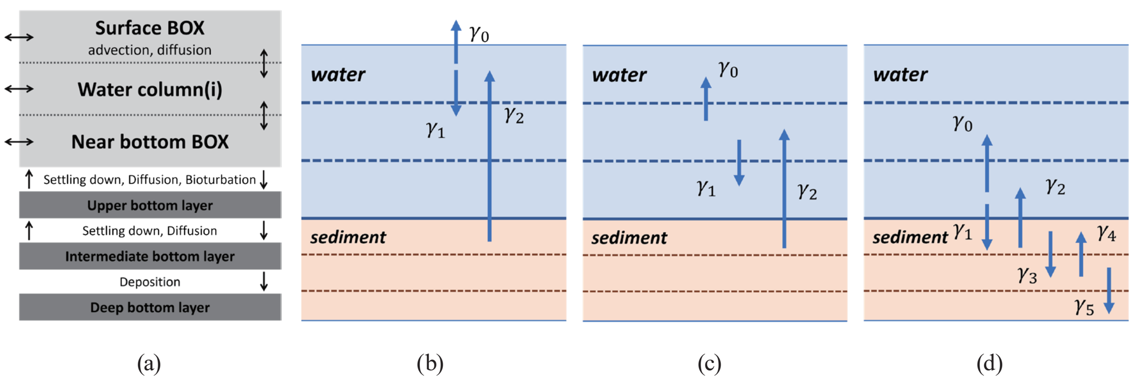

Fig. 1. (Color online) Schematic of transfer rates of radioactivity in POSEIDON-R: (a) vertical structure, (b) surface layer, (c) middle layer, and (d) bottom layer.

$$\frac{\partial C_{0ik}}{\partial t} = \sum_m \sum_j \left[\frac{F_{jimk}}{V_{0ik}} C_{0jm} - \frac{F_{ijkm}}{V_{0jm}} C_{0ik} \right] + \gamma_{0ik} C_{0(i+1)k} - \left(\gamma_{1ik} + \lambda\right) C_{0ik} + \frac{L_{t,k}}{h_{1k}} \gamma_{2k} C_{1k} + Q_{sik} \quad (1)$$

$$\frac{\partial C_{1k}}{\partial t} = -\left(\gamma_{2k} + \gamma_{3k} + \lambda\right) C_{1k} + \frac{h_{1k}}{L_{t,k}} \gamma_{1k} C_{01k} + \frac{L_{m,k}}{L_{t,k}} \gamma_{4k} C_{2k} \quad (2)$$

$$\frac{\partial C_{2k}}{\partial t} = -\left(\gamma_{4k} + \gamma_{5k} + \lambda\right) C_{2k} + \frac{L_{t,k}}{L_{m,k}} \gamma_{3k} C_{1k} \quad (3)$$

Here, C_0 denotes the radionuclide concentration (Bq/m^3) in the water column, while C_1 and C_2 represent the concentrations (Bq/m^3) in the surface and middle sediment layers, respectively. F refers to the water fluxes (t/yr), V is the box volume (m^3), and λ denotes the radioactive decay constant (yr^{-1}). Q_{sik} is the source of the activity (Bq/yr). L_t and L_m indicate the thicknesses (m) of the surface and middle sediment layers, respectively, and h_1 represents the depth (m) of the water column. The subscripts i and j correspond to water column layers, whereas m and k denote box numbers.

The parameters γ_0, γ_1, …, γ_5 represent the transfer rates of radionuclides between compartments, which are defined differently depending on the vertical position of the water column. To facilitate a clearer understanding of the transport pathways and roles of each variable, Figs. 1(b)–1(d) schematically illustrate the transfer processes occurring in the surface, middle, and bottom layers (including the sediment layer), respectively. The full mathematical formulation is described in Ref. 2.

2.2 Description of model forcing and input data

The model domain covers the marginal seas of the northwestern Pacific, including the Yellow Sea, the East China Sea, and the offshore regions east of the Korean Peninsula, and is divided into 176 boxes. This configuration is identical to that used by Maderich *et al.*(1) and Bezhenar *et al.*,(2) as shown in Fig. 2(a). Figure 2(b) shows an enlarged view of the region of interest around the Korean Peninsula. The water column is represented by three vertical layers: the upper layer (≤200 m), the middle layer (200–1000 m), and the deep layer (>1000 m). The number of layers varies depending on the local water depth.

Key input data for the system, such as inter-box water fluxes, boundary conditions, and the direct release of radioactive substances from FDNPP, were adopted from Ref. 2. The inter-box exchange rates were derived from the 10-year (2000–2009) simulation results of the Regional Ocean Modeling System (ROMS). The initial Cs-137 concentrations along the eastern and southern boundaries were determined using data from the Marine Radioactivity Information System (MARiS) database, as well as observational values reported by Kang *et al.*(5) and Nakano and Povinec.(6) Additionally, direct discharges of radioactive contaminants from the FDNPP into the ocean from 2011 to 2020 were incorporated, following the estimates provided by Povinec *et al.*(7)

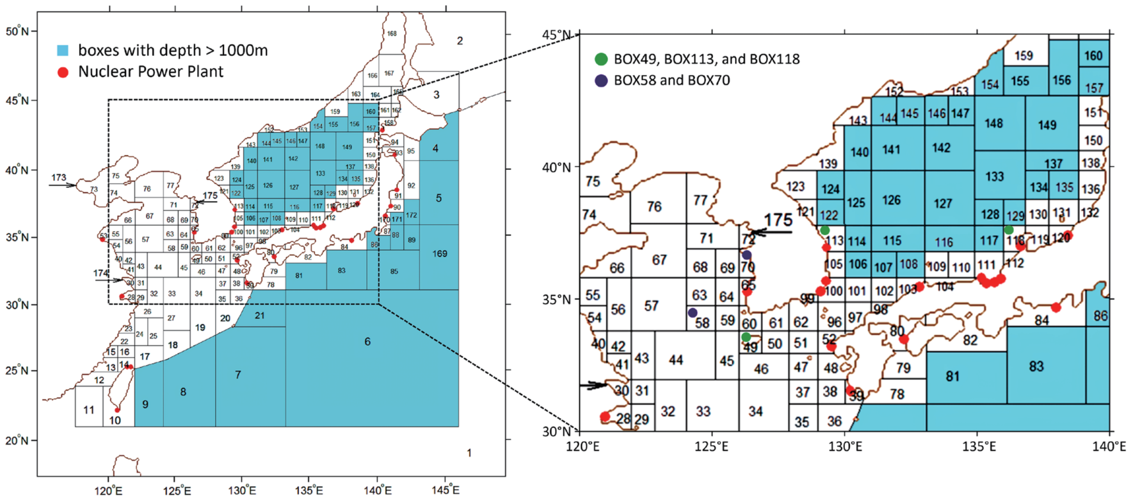

(a) (b)

Fig. 2. (Color online) (a) Overview of the model domain and (b) enlarged view of Korean Peninsula region with highlighted boxes analyzed in this study.

The atmospheric deposition of Cs-137 in this study was estimated using the 2D global annual fallout distribution data reconstructed on the basis of the methodology proposed by Tsumune *et al.*[8] While this study adopts the same assumption as Tsumune *et al.*[8]—that global fallout distribution is proportional to the spatial pattern of precipitation—the precipitation fields used for the reconstruction were taken from the Global Precipitation Climatology Project (GPCP) and the ERA reanalysis datasets. The box-specific deposition fluxes were calculated for the period from 1953 to 2000. For the period after 2000, the deposition data were updated using the datasets of Nakano[9] and Hirose *et al.*,[10] while the predicted deposition fluxes were further adjusted by applying radioactive decay corrections to the 5-year averaged fallout and boundary conditions. The final adjusted values were supplemented with predictions from the MATCH atmospheric transport model.[2]

The key physical parameters governing the exchanges between the water column and sediment layers in each box were estimated as realistically as possible on the basis of available observational data. These parameters include suspended sediment concentration, suspended sediment flux, bioturbation intensity, top sediment layer thickness, and porosity. Each parameter was re-evaluated primarily for the northwestern Pacific region (the main study area) and, where necessary, supplemented with relevant global observational datasets. A summary of these parameters is provided in Table 1.

The suspended sediment concentration was derived from the Level-2 satellite data (classification code 12; total suspended sediment, TSS, g/m^3) of the Geostationary Ocean Color Imager-II (GOCI-II) operated by the National Ocean Satellite Center (NOSC), Korea Hydrographic and Oceanographic Agency (KHOA). In the POSEIDON-R, suspended sediment concentrations are assigned for each box without considering temporal variability. In this study, the 2024 GOCI-II satellite data were used, and the mean values of observations on the 15th day of each month were applied. Spatial averaging was performed by calculating the mean TSS within a 0.5° radius around the center of each model box.

Table 1
Summary of key physical parameters used in the model.

Parameter	Method/data source	Reference
Suspended sediment	Total Suspended Sediment (TSS) product	GOCI-II Level2
Sediment flux	Sediment trap observations of suspended particle matter flux	Guo *et al.*(11); NCEI(12)
Bioturbation intensity and top sediment layer thickness	Mean values derived from global observation (1864–2018)	Solan *et al.*(13)
Porosity	Global seafloor porosity distribution estimated using machine learning techniques	Martin *et al.*(14)

Cs-137 exists primarily in a dissolved form in seawater but can also attach to clay minerals or organic matter, forming particulate phases capable of settling. In the POSEIDON-R model, the sediment flux is defined as the product of suspended sediment concentration and settling velocity ($SSW = W_g \times SS$), and in this study, sediment flux input values were derived using observed sediment flux data. For the Yellow and East China Seas, sediment flux data from Guo *et al.*(11) were used, while for other regions, global sediment trap (TMF) data provided by the National Centers for Environmental Information(12) under NOAA were utilized to estimate box-specific sediment fluxes. Figure 3 illustrates the relationship between suspended sediment concentration and sediment flux, along with the associated linear regression results and regression equation. Separate analyses (P2 LR) were conducted using the datasets from Guo *et al.*(11) and NCEI individually, as well as combined observations for comparison (P1 LR). Similar to the suspended sediment concentration, each physical parameter was assigned a single representative value for each model box.

Solan *et al.*(13) compiled a global metadata database on bioturbation and sediment mixing depth based on published studies and observational data collected worldwide from 1864 to 2018. The database contains 1281 bioturbation records and 1780 sediment mixing depth records, with region-, season-, and depth-specific summaries presented in tabular form. Because direct observations in the northwestern Pacific, the focus area of this study, are limited, the averages by depth range were adopted as model input parameters. In this study, the sediment mixing depth values were used to represent the top sediment layer thickness in the POSEIDON-R model. Specifically, the data were divided into three depth intervals, and the corresponding averages applied in the model are summarized in Table 2.

Direct observations of seafloor porosity are limited owing to the high cost of field measurements and the constraints of marine observation environments. Although Solan *et al.*(13) provided partial porosity information along with bioturbation and sediment mixing depth data, the number of records was insufficient for this study. Therefore, porosity data predicted by Martin *et al.*(14) using a machine learning approach were employed. Their study estimated global seafloor porosity distributions at a spatial resolution of 5 arc min (approximately 9 km) based on about 2000 surface sediment (upper 1 m) samples and various geomorphological, geological, and physical parameters. The dataset, available through Pangaea.de, excludes samples from geologically anomalous areas such as volcanic or rocky regions. Within the northwestern Pacific model domain, the porosity ranges from 0.5 to 0.8.

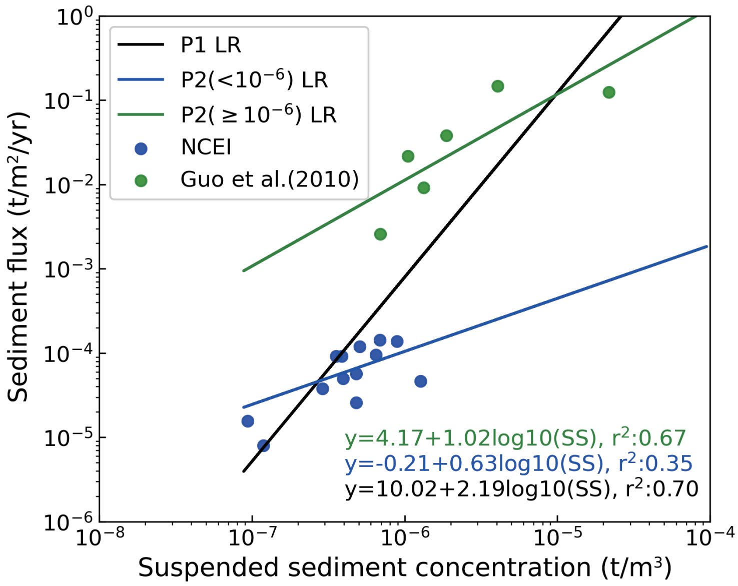

Fig. 3. (Color online) Relationship between suspended sediment concentration and sediment flux based on observational data.

Table 2
Depth-dependent variations in bioturbation intensity and top sediment layer thickness.

Parameter	<200 m	200–1000 m	>1000 m
Bioturbation intensity (m^2/yr)	4.25×10^{-3}	1.59×10^{-3}	5.23×10^{-4}
Top sediment layer thickness (L_t, m)	4.12×10^{-2}	6.25×10^{-2}	7.97×10^{-2}

2.3 Distribution coefficient (K_d) of Cs-137 observed in the eastern coast of Korea

KIOST conducted a series of studies to investigate the behavior of radionuclides in various marine environmental media. These investigations derived the K_d values of three radionuclides—Cs-137, Sr-90, and Pu-239240—for both the seawater-suspended particulate and seawater–sediment phases. In the present study, only the seawater–sediment K_d values of Cs-137 were utilized. Seawater and surface sediment samples were collected from five coastal stations adjacent to the Hanul Nuclear Power Plant (NPP) in 2023 (Zone-1 in Fig. 4) and from five deep-sea stations in the East Sea in 2024 (Zone-2 in Fig. 4). The resulting Cs-137 K_d values are summarized in Table 3, where values in parentheses denote the mean ± standard deviation (*SD*).

Prior to the K_d assessment, the seawater concentrations observed in Zone-1 were verified to fall within the range reported by the Korea Institute of Nuclear Safety (KINS), based on 17 years (2005–2022)[15] of long-term monitoring conducted near the Hanul NPP. This consistency corroborates the reliability and applicability of the observational dataset employed in this study. As summarized in Table 3, the mean Cs-137 K_d estimated for Zone-2 was 6214 ± 2128, which is more than six times higher than the coastal K_d of 1016 ± 365 obtained for Zone-1. This pattern

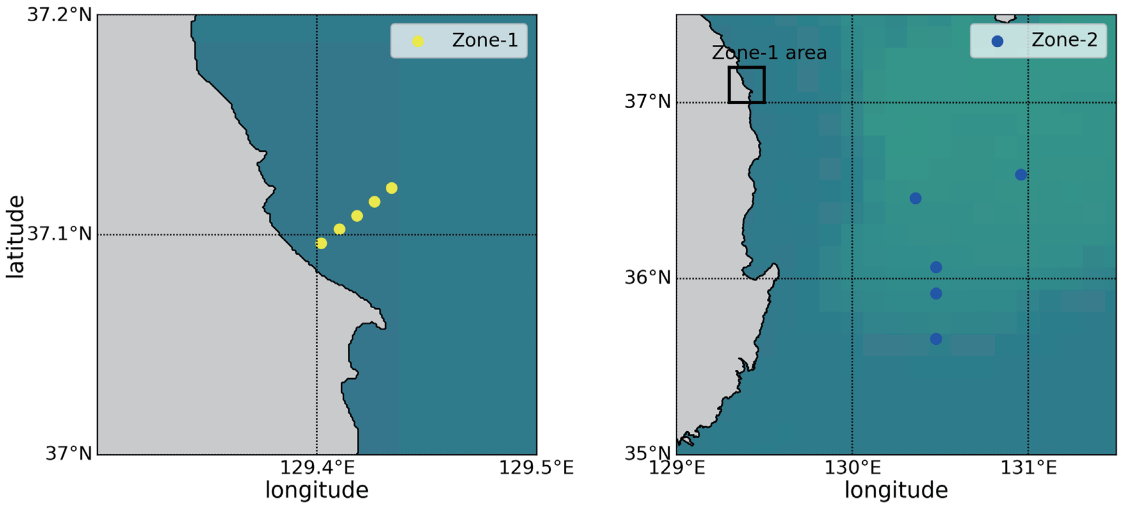

Fig. 4. (Color online) Locations for seawater and surface sediment sampling for K_d analysis: (a) Zone-1 and (b) Zone-2.

Table 3
Distribution coefficient (K_d) of Cs-137 in East Sea.

Radionuclide	Zone-1	Zone-2
Cs-137	600–1476 (1016 ± 365)	4162–9764 (6214 ± 2128)

contrasts with the general tendency for K_d to decrease with increasing water depth. In this study, emphasis was placed on incorporating the observation-based K_d values into the numerical simulations rather than diagnosing the underlying mechanisms.

The POSEIDON-R model applies K_d by distinguishing between *Local* (shallower than 200 m) and *Regional* (deeper than 200 m) water depths. In the default configuration, the model adopts the IAEA-recommended K_d values of Cs-137, set to 3000 for *Local* and 2000 for *Regional*. In this study, these default settings were replaced by observational values: the Zone-1 coastal K_d was applied to the local domain and the Zone-2 deep-sea K_d was applied to the regional domain.

2.4 Observational datasets used for model validation

To validate the model results, various observational datasets produced by domestic and international organizations were collected, standardized, and integrated into a unified database. The data were categorized by source institution and converted into a consistent format. Among these, the IAEA's MARiS and the Environmental Radioactivity Research Network Center (ERAN) database managed by the University of Tsukuba served as the primary data sources. In addition, radioactivity monitoring data for the surrounding sea of Korea were incorporated from KINS and KIOST. A summary of the datasets and their sources is provided in Table 4.

Table 4
Summary of observational data compiled for model validation.

Organization	Information
KINS	Regularly published reports (2005–2021) https://nsic.nssc.go.kr/marine/marineMonitoring.do
KIOST	Irregular monitoring in Korean coastal water since 2011
ERAN Database	HAMGlobal2021(1953–2021), HAMGlobal2022(1972–2020) https://www.ied.tsukuba.ac.jp/database/
MARiS	Global database operated by IAEA https://maris.iaea.org/explore

The IAEA-MARiS database(16) was established to monitor the long-term distribution of marine radionuclides worldwide and to compile the data related to nuclear weapons testing, NPP accidents, and other radiological events. In this study, observational data for seawater, sediments, suspended matter, and marine biota were obtained from MARiS. The dataset includes both literature-based and national monitoring data.

The ERAN database(17) of the University of Tsukuba compiles and manages global observational data on artificial radionuclides across various environmental media. Two datasets were used in this study: HAMGlobal2021 (covering 1953–2021) and HAMGlobal2022 Sediment (covering 1972–2020).

KINS conducts the annual monitoring of marine radioactivity in Korean coastal and offshore water at 78 stations extending up to 300 km from the shoreline.(18) The monitoring includes analyses of radionuclide concentrations in seawater, marine biota, and sediments. In this study, data from 2005 to 2021 were utilized. Additionally, the radioactivity survey data collected by KIOST since 2011 in Korean coastal and adjacent seas, including measurements of Cs-137, Sr-90, and Pu-239240, were also incorporated.

3. Simulation Results and Sensitivity Tests

In this section, the model performance was evaluated under modified conditions of atmospheric deposition and key physical parameters. The analysis revealed that the model was highly sensitive to the sediment flux, prompting additional sensitivity experiments, the results of which are also presented.

3.1 Simulation results and validation

In this section, the results obtained after recalculating atmospheric deposition and modifying key physical parameters are presented. The numerical simulations were compared for representative boxes located along the eastern coast of Korea (BOX113), around Jeju Island (BOX49), and along the Japanese coast (BOX118). For reference, the results of Bezhenar *et al.*(2) were included to evaluate the improvements achieved in this study. In addition, to examine the effect of K_d observed in the East Sea, supplementary simulations incorporating this parameter were also conducted.

Table 5 shows the default and adjusted physical parameters applied to BOX49, BOX113, and BOX118. The modified parameters include changes to sediment flux, suspended sediment concentration, bioturbation intensity, top sediment layer thickness, and porosity. In all three boxes, the sediment flux and bioturbation values were substantially increased, while the porosity and top sediment layer thickness were slightly reduced compared with the default settings. These adjustments were made to better represent the sediment–water interaction processes inferred from observational datasets.

Figures 5–7 show the comparison between the simulated and observed Cs-137 concentrations in the water column and sediments for each box. The simulations using the modified parameters (M0P1, M0P1Kd; red lines) were compared with those using the default parameters (2016, 2016Kd; black lines). In the water column, the improved cases (M0P1 and M0P1Kd) demonstrated slightly better agreement with the observed data, especially in the recent period after 2010.

More significant differences were observed in the sediment layer. The previous simulations generally overestimated Cs-137 concentrations, whereas the modified experiments reproduced the observed levels more accurately. Despite limited sediment observations in BOX49, the updated results show a clear improvement in reproducing the temporal decay trend.

Table 5
Default and adjusted physical parameters used for BOX49, BOX113, and BOX118.

Parameter	Box #					
	BOX49		BOX113		BOX118	
	default	modified	default	modified	default	modified
Sediment flux (t/m^{2}yr)	1.50×10^{-4}	9.76×10^{-5}	1.50×10^{-4}	4.29×10^{-4}	1.50×10^{-4}	2.57×10^{-4}
Suspended sediment (t/m^3)	6.00×10^{-6}	3.83×10^{-7}	6.00×10^{-6}	7.54×10^{-7}	6.00×10^{-6}	5.96×10^{-7}
Bioturbation intensity (m^2/yr)	3.60×10^{-5}	4.25×10^{-3}	3.60×10^{-5}	1.59×10^{-3}	3.60×10^{-5}	1.59×10^{-3}
Top sediment layer thickness (m)	1.00×10^{-1}	4.12×10^{-2}	1.00×10^{-1}	6.25×10^{-2}	1.00×10^{-1}	6.25×10^{-2}
Porosity	7.50×10^{-1}	5.59×10^{-1}	7.00×10^{-1}	6.72×10^{-1}	7.00×10^{-1}	5.43×10^{-1}

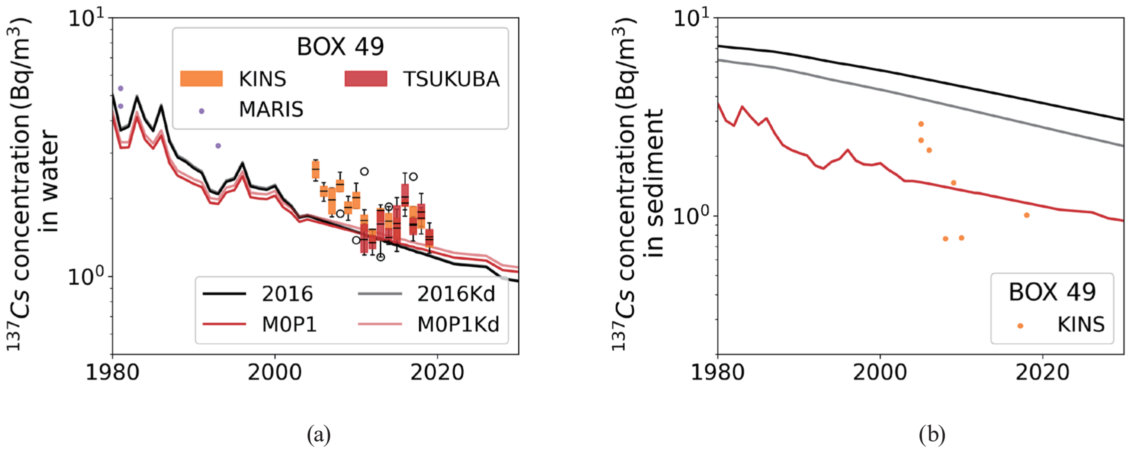

Fig. 5. (Color online) Comparison between simulated and observed Cs-137 concentrations in the (a) water column and (b) sediment in BOX49.

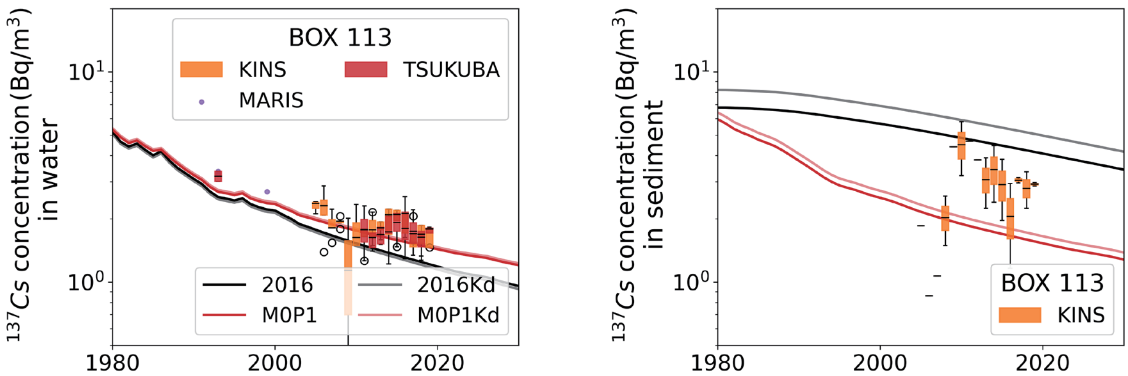

(a) (b)

Fig. 6. (Color online) Comparison between simulated and observed Cs-137 concentrations in the (a) water column and (b) sediment in BOX113.

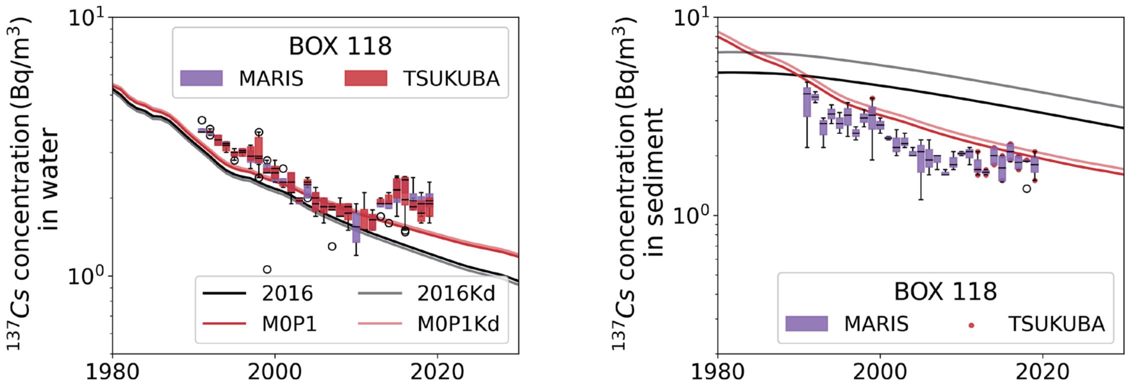

(a) (b)

Fig. 7. (Color online) Comparison between simulated and observed Cs-137 concentrations in the (a) water column and (b) sediment in BOX118.

For BOX113 and BOX118, located along the eastern coast of Korea and the Japanese coast, respectively, the M0P1(Kd) simulations slightly underestimated the observed values in BOX113 while showing a mild overestimation in BOX118. Nevertheless, the overall temporal patterns were reproduced more accurately than in the default simulations. These results suggest that the adjustments to sediment flux and associated physical parameters improved the model performance, particularly in representing the accumulation and retention of radionuclides in the sediment layer.

3.2 Sediment flux sensitivity analysis: experimental design and results

In this section, it was found that, unlike the results for the boxes located around Jeju Island and along the eastern coast of Korea and the western coast of Japan, the simulated Cs-137 concentrations in both the water column and sediment layers were underestimated in the Yellow and East China Sea boxes when the improved input parameters were applied. To address this discrepancy, additional sensitivity experiments focusing on the sediment flux term were conducted, and their results are presented. Although the model tended to underestimate concentrations across the broader Yellow and East China Sea regions, the analysis focused primarily on the Yellow Sea where observational data were available.

Table 6 shows the default and modified values of the key physical parameters applied to BOX58 and BOX70. In the modified experiments, the sediment flux values were increased by approximately 10 times for BOX58 and more than 30 times for BOX70, based on observational data from the Yellow Sea and using the P1 LR relationship shown in Fig. 3 of Sect. 2.2. The other parameters, including suspended sediment concentration, bioturbation intensity, top sediment layer thickness, and porosity, were also modified, and their adjusted ranges are comparable to those applied to BOX49, BOX113, and BOX118.

Figure 8 presents the comparison between the modeled and observed Cs-137 concentrations in the water column and sediment layers for BOX58 and BOX70, including the results from the sensitivity experiments. As in the previous section, black lines represent simulations using the default parameters (2016 and 2016Kd), whereas red lines indicate simulations using the improved parameters (M0P1 and M0P1Kd). The baseline simulations reasonably reproduced Cs-137 concentrations in the water column but tend to overestimate those in the sediment. In contrast, when the improved parameters were applied, BOX58 and BOX70 showed a general underestimation of Cs-137 concentration in both the water column and sediments compared with the observations.

To quantitatively analyze these results, three additional sensitivity experiments (M0P1, M0P2, and M0P3) were conducted using different parameterizations of sediment flux, as summarized in Table 7. In particular, the M0P3 experiment applied separate treatments of sediment flux for the water column and the sediment layer. In the water column, sediment flux was estimated on the basis of observational data, whereas in the sediment layer, it was defined by assuming a settling velocity of 0.3 m/yr in accordance with the formulation of sediment flux.

The results of these sensitivity experiments are also shown in Fig. 8, where M0P2(Kd) is indicated by blue lines and M0P3(Kd) by green lines. The M0P2 experiments, which applied a linear relationship derived for the suspended sediment concentration around 10^{-6} t/m^3, showed partial improvement but still tended to underestimate Cs-137 concentrations in both the water

Table 6
Default and adjusted physical parameters used for BOX58 and BOX70.

Parameter	Box #			
	BOX58		BOX70	
	default	modified	default	modified
Sediment flux (t/m^{2}yr)	1.50×10^{-4}	1.71×10^{-3}	7.50×10^{-4}	2.72×10^{-2}
Suspended sediment (t/m^3)	6.00×10^{-6}	1.42×10^{-6}	1.00×10^{-5}	5.09×10^{-6}
Bioturbation intensity (m^2/yr)	3.60×10^{-5}	4.25×10^{-3}	3.60×10^{-5}	4.25×10^{-3}
Top sediment layer thickness (m)	1.00×10^{-1}	4.12×10^{-2}	1.00×10^{-1}	4.12×10^{-2}
Porosity	7.50×10^{-1}	5.16×10^{-1}	7.00×10^{-1}	5.98×10^{-1}

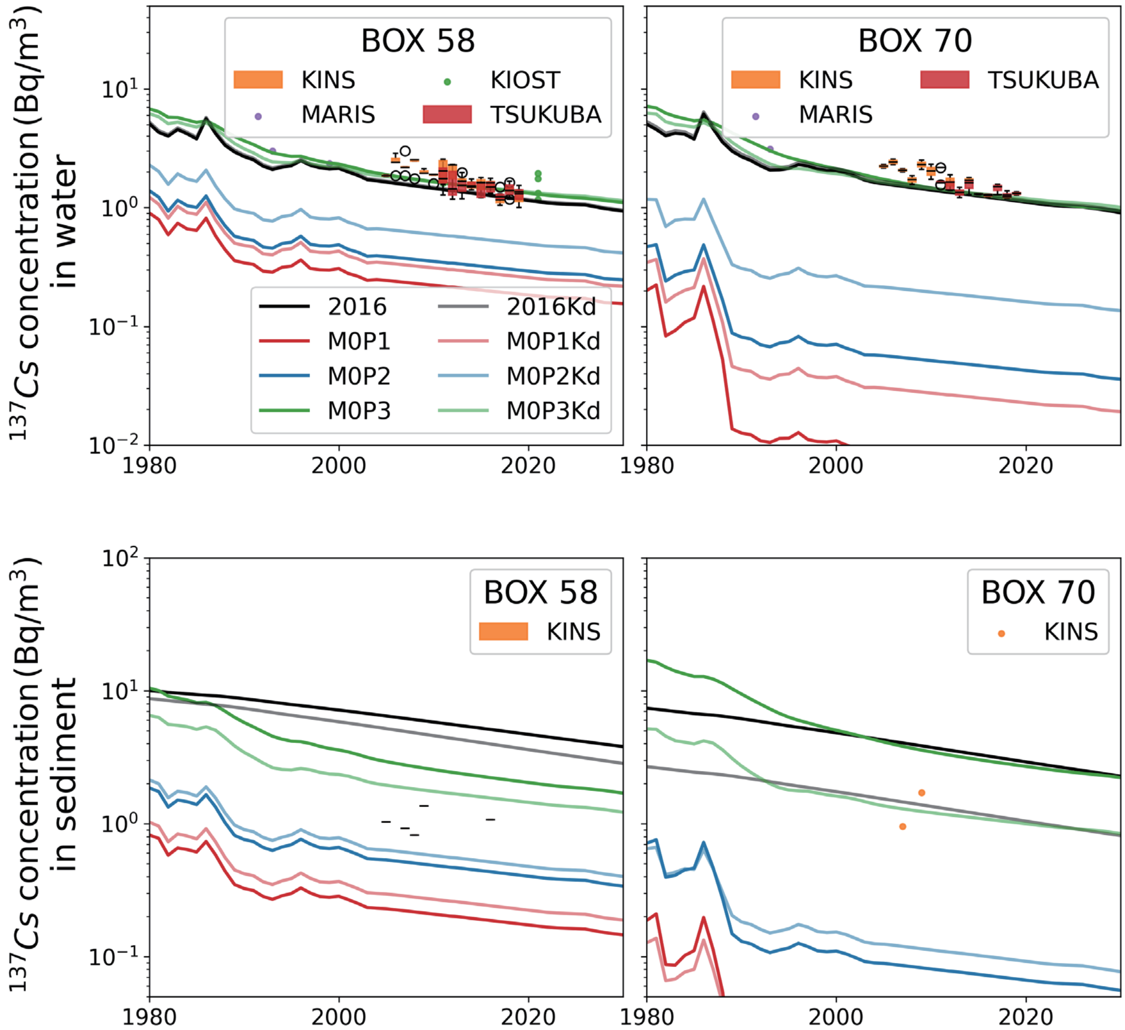

Fig. 8. (Color online) Comparison of modeled and observed Cs-137 concentrations in the water column and sediment layers for BOX58 and BOX70, including sensitivity experiment results.

Table 7
Sensitivity experiments for sediment flux (refer to Fig. 3).

Experiment	Condition	
	Sediment flux	
	Water column	Sediment
M0P1	P1 LR	P1 LR
M0P2	P2 LR	P2 LR
M0P3	P2 LR	modified SS × 0.3 m/yr

column and sediments. In contrast, the sediment simulations showed a significant improvement in model reproducibility. The simulated Cs-137 concentrations in the water column closely matched the observations, while those in the sediments were slightly overestimated but reproduced the overall temporal trends most accurately.

4. Discussion on the Effects of Sediment Flux and K_d on Model Performance

The simulation results of this study showed that the POSEIDON-R model generally reproduced the temporal variations in Cs-137 concentration in both seawater and sediments; however, the model performance differed by region. These regional discrepancies are interpreted to arise from differences in sediment flux and the physical processes governing sediment–water exchange in each area.

In BOX49, BOX113, and BOX118, the agreement between the modeled and observed concentrations improved when the atmospheric deposition and key physical parameters—particularly sediment flux, suspended sediment concentration, and bioturbation intensity—were revised. The simulations using the updated input data (M0P1, M0P1Kd) alleviated the overestimation of sedimentary Cs-137 concentrations found in the baseline simulations (2016, 2016Kd) and more accurately reproduced the observed decreasing trend over time. These improvements indicate that adjusting the physical parameters to reflect region-specific sediment–water interactions is effective for enhancing model reproducibility.

In contrast, in the Yellow Sea (BOX58 and BOX70), the same revised parameters resulted in the overall underestimation of Cs-137 concentrations in both the water column and sediments. This behavior is attributed to the characteristic environment of the Yellow Sea, which is shallow, exhibits active resuspension, and has intense sediment–water exchange processes.(11) The observed sediment fluxes are considerably larger in the Yellow Sea than in other regions, and resuspension rates are also reported to be high. However, the current POSEIDON-R model does not adequately account for resuspension from sediments back into the water column and assumes a single sediment flux for both the water column and the sediment layer. As a result, Cs-137 is transported very rapidly from the water column to the sediment layer and is excessively accumulated in deeper sediment layers within the model.

To address these limitations, additional sensitivity experiments (M0P1–M0P3) targeting the sediment flux term were conducted. The results demonstrated that the POSEIDON-R model is highly sensitive to changes in sediment flux (as seen between M0P1 and M0P2), and that separating the sediment flux between the water column and the sediment layer (M0P3) substantially improved the model performance. In the M0P3 experiment, the simulated Cs-137 concentrations in the water column were closely aligned with observations, and although the concentrations in the sediment layer were slightly overestimated, the overall temporal trend was reproduced most accurately. These findings suggest that using different settling velocities for the water column and the sediment layer provides a more realistic representation of the physical environment. This approach is particularly important in high-turbidity and high-resuspension regions such as the Yellow Sea.

Furthermore, the sensitivity analysis showed that the model's response to variations in distribution coefficient (K_d) was significantly greater in the Yellow Sea than in the eastern coast of Korea and the Japanese coastal region. This indicates that the interaction between settling velocity and K_d plays a crucial role in determining the partitioning of Cs-137 between the dissolved and particulate phases. In other words, the adsorption and desorption processes within the sediments strongly affect the long-term retention and accumulation of Cs-137, and these processes vary depending on regional physical characteristics. Therefore, the accurate regional calibration of both K_d and sedimentation velocity is essential for precisely simulating the long-term behavior of radionuclides in marine sediments. Moreover, further improvement may be achieved by distinguishing between the dissolved–particulate K_d and the water–sediment K_d when applying distribution coefficients in the model.

Overall, these results indicate that region-specific sedimentary environments are major controlling factors governing the transport and long-term distribution of radionuclides in the marine environment. In particular, spatial variability in settling velocity, resuspension intensity, sediment exchange, and particulate flux plays a critical role in shaping radionuclide behavior. To further enhance the predictive capability of the POSEIDON-R model, future work should incorporate refined region-specific parameterizations of particle dynamics, implement separate modules for resuspension and settling processes, and apply distinct K_d values for water-suspended particles and water–sediment interactions.

5. Conclusions

In this study, the POSEIDON-R model was applied to simulate the long-term behavior of Cs-137 in the East Sea, the waters around Jeju Island, the Japanese coastal region, and the Yellow Sea using updated observational data and revised physical parameters. The results showed that, in the East Sea and the Jeju–Japan coastal regions, the application of improved input parameters reduced the previous overestimation of sedimentary Cs-137 and more realistically reproduced the temporal evolution of concentrations. These improvements indicate that region-specific adjustments to sediment–water interaction parameters are effective in enhancing model performance.

In contrast, in the Yellow Sea, the same parameter set resulted in an overall underestimation of Cs-137 concentrations in both the water column and sediments. This discrepancy was attributed to the unique sedimentary environment of the Yellow Sea, characterized by small depth and high resuspension rates, which is not fully represented in the default model configuration. Additional sensitivity experiments focusing on sediment flux revealed that the M0P3 experiment, which applied different settling velocities to the water column and sediment layer, provided the best agreement with observations. Furthermore, the model showed particularly high sensitivity to variations in K_d in this region, confirming that the accurate regional K_d estimation and improved parameterization of settling and resuspension processes are critical for enhancing model predictive capability.

This study also provides several methodological advances to the POSEIDON-R framework: (1) separating the settling velocities for suspended and deposited particles, which had not been implemented in previous studies; (2) quantitatively demonstrating, for the first time, the importance of flux parameterization in resuspension-dominant systems such as the Yellow Sea; and (3) evaluating the impact of observed, region-specific K_d values, thereby offering a novel contribution to improving radionuclide model accuracy. These results further emphasize the critical role of sensor-derived observations, satellite remote sensing products, and advanced marine monitoring approaches in enhancing model parameterization and predictive accuracy for marine radionuclide transport.

Acknowledgments

The authors thank the editor and reviewers for their useful comments and suggestions that helped us considerably. This research was supported by the Korea Institute of Marine Science and Technology Promotion (KIMST) funded by the Ministry of Oceans and Fisheries, Republic of Korea (RS-2023-00256141, Development of a Global Marine Radioactive Contamination Effect Prediction System).

References

1 V. Maderich, R. Bezhenar, R. Heling, G. de With, K. T. Jung, J. G. Myoung, Y.-K. Cho, F. Qiao, and L. Robertson: J. Environ. Radioact. **131** (2014) 4.
2 R. Bezhenar, K. T. Jung, V. Maderich, S. Willemsen, G. de With, and F. Qiao: Biogeosci. Discuss. **13** (2016) 3021.
3 V. Maderich, R. Bezhenar, Y. Tateda, M. Aoyama, D. Tsumune, K. T. Jung, and G. de With: MethodsX **5** (2018) 1251.
4 H. Kim, K. O. Kim, S. Seo, Y.-I.]
Kim, and M. Lee: KIOST Technical Report TR-2025-0561 (KIOST, Busan, 2025). https://doi.org/10.22808/TR-2025-0561 (in Korean).
5 D.-J. Kang, C. S. Chung, S. H. Kim, K.-R. Kim, and G. H. Hong: Mar. Pollut. Bull. **35** (1997) 7.
6 M. Nakano and P. P. Povinec: Deep Sea Res. Part II **50** (2003) 2803.
7 P. P. Povinec, K. Hirose, and M. Aoyama: Radioactivity Impact on the Environment (Elsevier, USA, 2013) Chap. 4.
8 D. Tsumune, F. O. Bryan, K. Lindsay, K. Misumi, T. Tsubono, and M. Aoyama: Mar. Pollut. Bull. **197** (2023) 115663.
9 M. Nakano: Radioactivity in the Environment 8, P. P. Povinec and J. A. Sanchez-Cabeza, Eds. (Elsevier, Amsterdam, 2006) Chap. 9.
10 K. Hirose, Y. Igarashi, and M. Aoyama: Appl. Radiat. Isot. **66** (2008) 1675.
11 X. Guo, Y. Zhang, F. Zhang, and Q. Cao: Deep Sea Res. Part II **57** (2010) 1058.
12 Global compilation of sinking particle data collected by sediment trap studies (NCEI Accession 0210959): https://www.ncei.noaa.gov/access/metadata/landing-page/bin/iso?id=gov.noaa.nodc:0210959 (accessed April 2025).
13 M. Solan, E. R. Ward, E. L. White, E. E. Hibberd, C. Cassidy, J. M. Schuster, R. Hale, and J. A. Godbold: Sci. Data **6** (2019) 58. https://doi.org/10.1038/s41597-019-0069-7
14 K. M. Martin, W. T. Wood, and J. J. Becker: Geophys. Res. Lett. **42** (2015) 10640. https://doi.org/10.1002/2015GL065279
15 KINS report: https://nsic.nssc.go.kr/marine/marineEnvRadReport.do (accessed January 2025).
16 IAEA-MARIS database: https://maris.iaea.org/explore (accessed January 2025).
17 ERAN database: https://www.ied.tsukuba.ac.jp/database/ (accessed January 2025).
18 KINS monitoring information: https://nsic.nssc.go.kr/marine/marineMonitoring.do (accessed April 2025).

About the Authors

Hanna Kim received her M.S. degree in coastal engineering from Seoul National University in 2007; she is currently working at the Korea Institute of Ocean Science & Technology (KIOST). Her research interests include the box modeling of radionuclides and wave modeling. (sarah314@kiost.ac.kr)

Seongbong Seo received his Ph.D. degree in oceanography from the University of Science and Technology (UST) and is currently a senior research scientist in the Ocean Circulation and Climate Research Division at KIOST. His research interests include ocean dispersion modeling and artificial intelligence applications. (sbsoeo@kiost.ac.kr)

Kyeong Ok Kim received his Ph.D. degree from Kyoto University and is currently a principal research scientist in the Ocean Circulation and Climate Research Division at KIOST. His research interests include coastal hazard modeling and atmosphere–ocean interactions. (kokim@kiost.ac.kr)

Young-Il Kim received his Ph.D. degree from the University of Hokkaido and is currently a principal research scientist in the East Sea Research Institute at KIOST. His research interests include the material transport process in the ocean. (yikim@kiost.ac.kr)

Myoung Hoon Lee graduated from Pukyong National University in 2015 and is currently working at KIOST. His research interests include the analysis of various chemical elements in the ocean. (leemh@kiost.ac.kr)

Hyun-Gyu Lim received his Ph.D. degree in climate dynamics from Pohang University of Science and Technology (POSTECH) and is currently a senior research scientist in the Ocean Circulation and Climate Research Division at KIOST. His research interests include ocean biogeochemical modeling and the high trophic level of the marine ecosystem. (hglim@kiost.ac.kr)